Colloid Polym Sci (2007) 285:1067–1075
DOI 10.1007/s00396-007-1649-1

ORIGINAL CONTRIBUTION

Thermal transitions in associating aqueous block copolymers: light scattering, rheology and spectroscopy

Silvia Pede · Luciano Galantini · Camillo La Mesa · Donatella Capitani · Anna Laura Segre

Received: 13 November 2006 / Accepted: 15 January 2007 / Published online: 17 February 2007

Abstract Solutions containing a polyoxy-ethylene/polyoxy-propylene/polyoxy-ethylene (PEO–PPO–PEO) block copolymer, indicated as F68, in water were investigated as a function of composition and temperature. Hydrogen nuclear magnetic resonance (^{1}H NMR) line width, chemical shift, self-diffusion, spin-lattice relaxation times, laser light scattering and rheological methods were used. The monomer–micelle equilibrium and the micelle–liquid crystalline phase transitions depend on the F68 content in the mixture and temperature. Significant changes in light scattering intensity and apparent hydrodynamic radius are associated to micelle formation above the critical micellar temperature (CMT). According to a Contin analysis, this behaviour is reflected in the presence of two populations in the intensity–intensity autocorrelation functions. The contributions due to molecules and micelles can be evaluated separately. No such effects are observed below the CMT. Micelle onset is also associated to variations in ^{1}H NMR spectra, affecting the chemical shift, line width and spin-lattice relaxation time of the PPO methyl protons and self-diffusion, as well. Spin-lattice relaxation times of PEO chains, conversely, change significantly at temperatures close to the micelle–liquid crystalline thermal transition. Similar results were obtained from the line width of ^{2}H NMR spectra as a function of *T*. Significant changes in both viscous and elastic modulus were also observed and ascribed to PPO dehydration, at the CMT, as well as to squeezing and dehydration of PEO units in liquid crystal formation, respectively.

Keywords Block copolymers · Micelles · Liquid crystals · Phase transitions · NMR relaxation times · NMR self-diffusion · Light scattering · Rheology

S. Pede · L. Galantini · C. La Mesa (✉)
Dipartimento di Chimica,
Università degli Studi di Roma "La Sapienza",
P.le A. Moro 5,
00185 Rome, Italy
e-mail: camillo.lamesa@uniroma1.it

L. Galantini
e-mail: l.galantini@caspur.it

D. Capitani · A. L. Segre
Istituto di Chimica Nucleare, CNR,
Area della Ricerca di Roma,
CP 20 Monterotondo Stazione,
00016 Rome, Italy

Introduction

The molecular structure of Pluronics, Poloxamers and similar block copolymers consists in alternating sequence of polyoxy-ethylene (PEO) and polyoxy-propylene (PPO) or other lipophilic units [1]. Their physical state, solubility and phase behaviour are controlled by the overall molecular mass and by the weight percent of the PEO portion [2]. High polyoxy-ethylene content ensures significant water solubility, and vice-versa [3]. The above compounds adsorb at the air–water interface [4] and behave similarly to alkyl polyoxy-ethylene glycol surfactants, C_nEO_m [5, 6].

In proper conditions, block copolymers of the Pluronic family form up to seven different mesophases, plus normal and reverse solutions [7–10], as the interfacial curvature of their aggregates can be matched with continuity. The above features imply a significant temperature and concentration dependence of solute–solvent interactions, similar to those observed in C_nEO_m. Hydration–dehydration processes, in particular, can be significant. They are responsible for modifications in the chain packing and conformation of block copolymers and modulate phase transitions and other

supra-molecular association modes. The thermodynamics of micelle-like association for the above compounds is rationalised by assuming significant and selective dehydration of the different copolymer regions. Detailed studies on Pluronics hydration have been exhaustively described in selected papers [11, 12].

In the following, we report on a member of the Pluronics family, F68, and discuss the results obtained for this selected system by a wide variety of experimental methods as a function of composition and temperature. F68 has a high PEO/PPO ratio and is, thus, a strongly hydrophilic block copolymer compared to other block copolymers. It forms micellar and liquid crystalline structures as a function of temperature and composition.

Temperature has a pronounced effect on the supra-molecular association and phase transitions of block copolymers in solution [13]. The effect of temperature on the molecule–micelle equilibrium, as well as on transitions from micelles to viscous isotropic liquid crystalline phases (having a body-centered cubic structure, bcc, [14–16]) are the subject of this work. We report on and discuss in this paper the modifications in rheological, spectroscopic and light scattering (LS) properties associated with the aforementioned transitions. Hydrogen nuclear magnetic resonance (^{1}H and ^{2}H NMR) methods, together with static and dynamic LS measurements, were used to investigate the molecule–micelle equilibrium, while rheology and ^{1}H spin-lattice relaxation times (or ^{2}H line width) the micelle–liquid crystalline one.

The present results give information on the effect that temperature and composition have on the conformation of different regions in the polymer chain, on the role they play in the formation of organised phases and on hydration of F68. Some methods give the possibility to investigate collective effects (rheology, for instance); others are more sensitive to the molecular details underlying association and/or dehydration. The links between the local dynamics (obtained by ^{1}H spin-lattice relaxation times) and the macroscopic one (inferred by rheology) are briefly discussed.

Experimental section

Materials

F68, a PEO-PPO-PEO tri-block copolymer of molecular mass close to 8,400 D, (BASF), was used as received. The relative amount of PEO in the polymer is about 80% and the hydrophilic-lipophilic balance (HLB) value is high (i.e. the product is highly water-soluble). The HLB value is an empirical parameter, weighing the contribution of each molecular part in the surfactant or the block copolymer [17]. This PEO/PPO weight ratio corresponds to an average structural formula of EO_{76}-PO_{30}-EO_{76}. The melting temperature of F68, T_m (inferred by optical microscopy), is 58±0.5 °C. The viscosity of bulk F68, η_{bulk}, and of 1.00 F68% aqueous solution, η_{sol}, was measured by Ubbelohde viscometers. The related values are 1.003 centiPoise (cP) at 77.0 °C and 1.0324 cps, at 25.00 °C, respectively. Within the experimental data accuracy (1.0%), they are equivalent to those indicated by the purveyor [18].

Water was filtered, re-distilled over alkaline $KMnO_4$, deionised and degassed: Its conductivity (κ) at 25 °C is $\approx 5\times10^{-7}$ S m^{-1}. When required, it was replaced by D_2O, on a mole fraction basis. Differences in the transition temperatures associated with replacement of water with D_2O are 1–2 K.

The solutions were prepared by weight, equilibrated at room temperature until equilibrium was attained and stored in a refrigerator at 4 °C. The solutions for NMR experiments were prepared by weight into 5-mm i.d. glass tubes, which were flame-sealed and equilibrated at the required temperature before measurements were run.

Methods

Nuclear magnetic resonance

A Bruker AMX 600 unit, operating at 600.13 MHz on proton, was used. The residual monodeuterated HDO signal of water was not suppressed. A 90° pulse (duration, 10–11 ms) was followed by a 2.0 s delay, with an acquisition time of 2.2 s. This procedure ensures a complete spin relaxation. The spectral time domain (32 K points) was Fourier-transformed into a 16 K point spectrum. No phase adjustment was required. The line broadening was moderate, even at large F68%.

Spin-lattice relaxation times, T_1 (s), were measured by an 180°_y-τ-90°_x pulse sequence [19]. Sixteen different delay times were used for PEO protons and the methyl group in the PPO chain. The signal intensity, $I(t)$, was fitted according to

$$I(t) = I^\circ + P\exp\left(-\frac{t}{T_1}\right) \quad (1)$$

where I° is the unperturbed signal intensity, P a constant and t the measuring time. Strictly mono-exponential decays were observed on both C_2H_4 and CH_3 signals at all temperatures.

^{2}H NMR was performed at 92.12 MHz by the same instrument. Details on the apparatus setup and measuring procedures are reported elsewhere [20, 21].

^{1}H NMR self-diffusion was measured by a low-resolution unit, upgraded by Stelar, working at 15.0 MHz on protons. More details on the apparatus setup and on the

measuring procedures are reported elsewhere [22, 23]. The Stejskal–Tanner equation was used to get the self-diffusion coefficients, according to [24, 25]

$$I(2\tau, g) = I^{\circ} \exp\left[-\frac{2\tau}{T_2} - (\gamma g \delta)^2 \left(\Delta - \frac{\delta}{3}\right) D\right] \quad (2)$$

where I (2τ, g) is the signal intensity in presence of the gradient, τ and T_2 are the pulse width and the transverse relaxation time, respectively, γ the gyro-magnetic ratio of ^{1}H, g the field gradient strength, δ its duration, Δ the sequence repetition time and D the diffusion coefficient. The accuracy on NMR self-diffusion values is within 2–3%, when the temperature is kept constant to 0.1 °C.

Light scattering

A Brookhaven BI-2030 AT unit was used. The goniometer is a Brookhaven BI-200 SM one. An Argon ion laser, operating at 514.5 nm and 20 mW (to avoid heating) was used. Millipore 0.1-μm filters filtered the samples before performing LS measurements. More details on the apparatus setup, measuring procedures and data elaboration are reported elsewhere [26, 27]. The field temporal auto-correlation function, $g_1(\tau)$, was derived by [28]

$$g_2(\tau) = \frac{\langle I(t)/(t+\tau)\rangle}{\langle I(t)\rangle^2} = 1 + B|g_1(\tau)|^2 \quad (3)$$

where $g_2(\tau)$ is the intensity auto-correlation function and B an instrumental constant. To analyse $g_1(\tau)$, the following cumulant expansion was used:

$$\ln|g_1(\tau)| = -\Gamma_1\tau + \left(\frac{\Gamma_2}{2}\right)\tau^2 \quad (4)$$

where Γ_1 and Γ_2 are the first and second cumulant, respectively.

Rheology

A TA AR 100 stress-controlled instrument, working in cone-plate geometry, was used. It is equipped with a Peltier element, ensuring the constancy on temperature to ±0.02 °C. Information on the apparatus setup and on the measuring procedures are reported elsewhere [29, 30]. To avoid flow of the solutions during the measurements, the volume fraction of the disperse phase, Φ, is higher than 0.2 (22 F68%).

There G' is the elastic and G'' the loss modulus, respectively. They are the real and imaginary components of the complex visco-elastic modulus, G^*, see [31]. $G'(T)$ and $G''(T)$ values (Pa) were measured at a scan speed of 1 or 3 °C min^{-1}, keeping the angular frequency, ω (rad s^{-1}), fixed to 1, 3 or 6. The use of lower frequencies implies the occurrence of spurious effects in both G' and G'' values and was avoided.

The applied stress for creep tests was 5 Pa in solutions and 80 Pa in liquid crystalline samples, respectively. The recovery time is 6.0×10^2 s in the former and 1.2×10^3 s in the latter case. Care was taken to operate in the linear perturbation regime for both oscillatory and creep test measurements.

Results and discussion

Phase diagram

The liquid crystalline phase onset was determined by the apparent fluidity of the samples located in a water bath. No changes in optical birefringence are observed. The mobility of small glass balls (1 mm diameter) located in the tubes was used to determine the transition temperature, T_{tr}. The solution–liquid crystalline phase boundaries are subject to some uncertainties and to ±1.5 °C. The molecule–micelle equilibrium was investigated by LS, NMR and by rheology for copolymer content higher than 0.2 Φ. The transition from micelles to liquid crystals was investigated by NMR relaxation and rheology.

The phase diagram obtained by combining the above results is reported in Fig. 1. There is no significant difference between critical micellar temperatures (CMT) obtained from different experimental methods. The temperature at which changes in apparent self-diffusion, chemical shift and relaxation times occur are super-imposable and allow drawing the location of the CMT curve in Fig. 1. The molecule–micelle transition temperature drastically changes on increasing F68%, and reduces from about 50 (at 2.0%) to 35 °C (at 7.0%). Thereafter, it decreases much more smoothly.

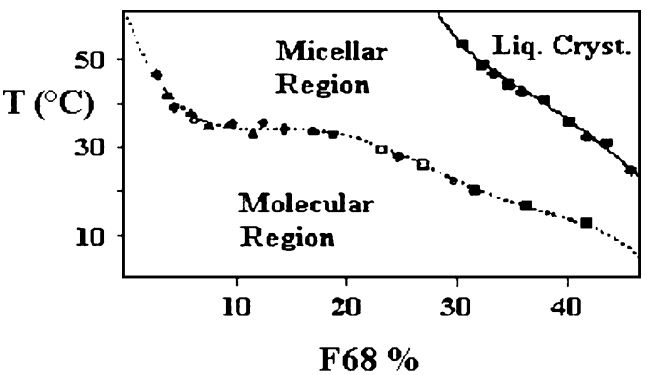

Fig. 1 Partial phase diagram of the water-F68 system, in the plane composition (F68%)-temperature (°C). The CMT, *dotted line*, was obtained by ^{1}H NMR chemical shift (*filled diamond*), relaxation (*open circle*), rheology (*open square*) and LS (*open rectangle*); the liquid crystalline phase border by visual observation, *full line*, ^{1}H NMR relaxation (*filled circle*) and rheology (*filled square*). The phase boundaries are to ±1.5 °C

The occurrence of uni-molecular species at low temperature and of micelles above a certain T threshold can be observed. The strong effect of temperature on micellar association implies the occurrence of significant entropic contributions because of an extensive release of hydrophobic hydration water [32–34]. This hypothesis is consistent with statements by Zhou and Chu [11, 12] as well as, for instance, by Fourier transform infrared, FT-Raman and electron paramagnetic resonance spectroscopy [35–37]. The release of two or three water molecules per PPO group implies a significant dehydration.

On increasing the temperature, concentrated F68 micellar solutions are transformed into a bcc mesophase [38, 39]. Micellar solutions are viscous (or visco-elastic), but the mesophase is elastic and does not allow trapped bubbles to escape [29, 30]. The mesophase is optically and magnetically isotropic. No deuterium quadrupole splitting or optical birefringence is concomitant to the phase onset. Perhaps, significant changes in ^{2}H transverse relaxation time of D_2O are associated to such transitions (Fig. 2).

Light scattering

To determine the mechanism causing the decay of the intensity auto-correlation function, Γ_1 is plotted as a function of the squared scattering vector, q^2. Linear fits in q^2 with an intercept close to zero characterize both the molecular and the micellar regimes, Fig. 3 and indicate that the dominating relaxation processes are due to translational diffusion.

The apparent diffusion coefficient of F68, D_{app}, was obtained by

$$D_{app} = \frac{\Gamma_1}{q^2} \tag{5}$$

The solute apparent hydrodynamic radius, R_{app}, was calculated from D_{app} values by the Stokes–Einstein equation. The dependence of R_{app} values on temperature is reported in Fig. 4. Close to the CMT, significant departures of R_{app} values from the low temperature behaviour occur.

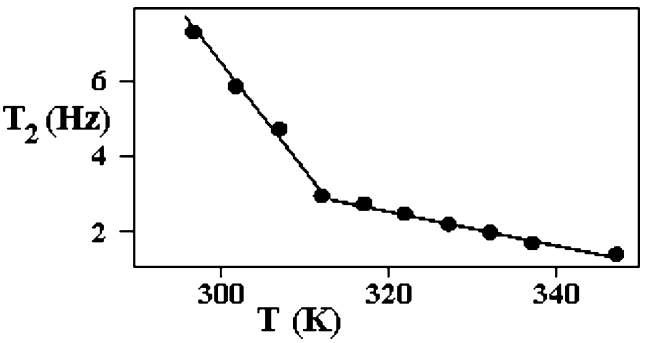

Fig. 2 Dependence of deuterium transverse relaxation time, T_2, in Hz, on temperature, in K, for a sample containing 45.03 F68% in D_2O. The *intersection point between lines* indicates the transition to a liquid crystalline phase

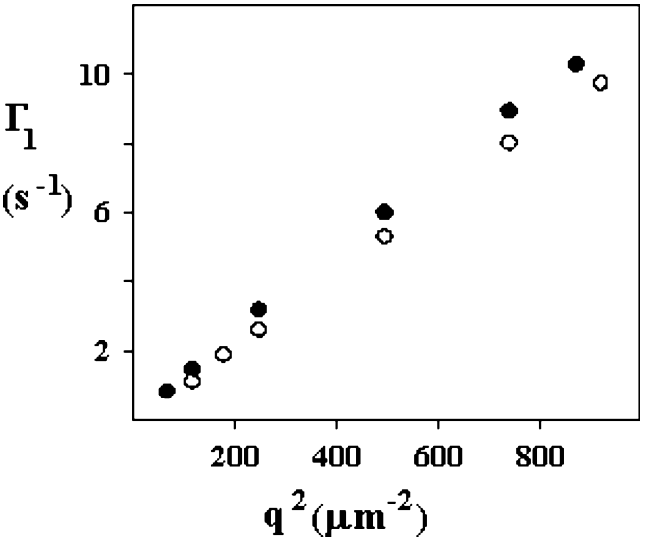

Fig. 3 Plot of Γ_1 (rad s^{-1}) vs the squared scattering vector q^2 (μm^{-2}) for a sample containing 4.98 F68% at 25.0 °C (*filled circles*), in molecular regime, and 45.0 °C (*open circles*), above the CMT

The light intensity scattered from the solution, corrected for the solvent contribution, is reported in Fig. 5. In agreement with R_{app} vs T plots, I is nearly constant at low temperatures and increases from the CMT upwards. Beyond a certain threshold (≈50 °C), R_{app} values are almost constant (Fig. 4), whereas I (Fig. 5) still grow on increasing T. According to the classical LS theory, I is related to the apparent mean molar mass, M_{app}.

Almgren et al. [40] reported LS measurements on Pluronic L 64. They found that small amounts of large, strongly scattering impurities affect the measurements.

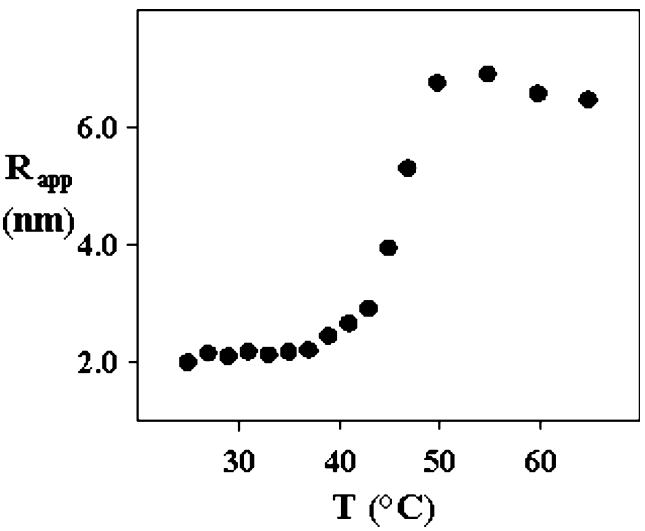

Fig. 4 Dependence of the average apparent hydrodynamic radius, R_{app}, (Å), for a 5.02 F68% solution, on T, (°C)

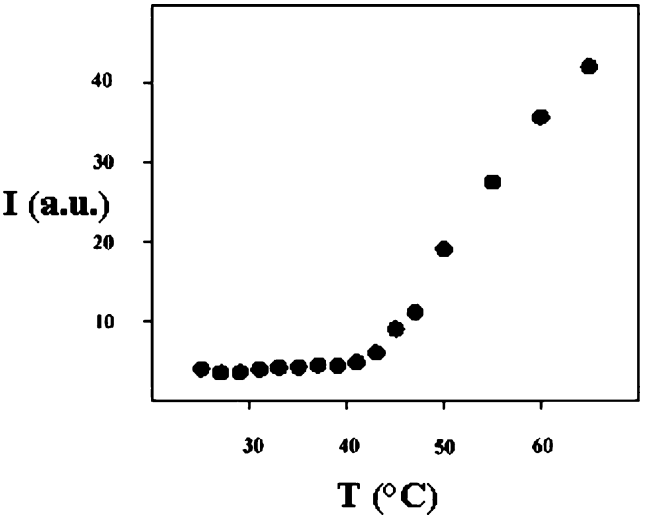

Fig. 5 Plot of the average light intensity scattered from a 5.02 F68% solution, I (a.u.), vs T (°C). Data are corrected for the solvent contribution

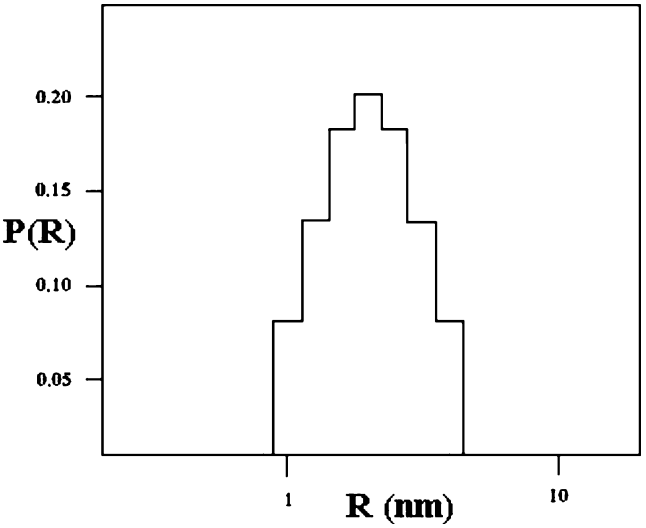

Fig. 6 The intensity weighted distribution, $P(R)$, in arbitrary units, as a function of R_{app}, in nm, well below the CMT, in molecular form. The solution contains 4.85 F68%

Below the CMT, they observed that the intensity correlation function is the sum of a strong intensity-weighted contribution, due to the impurities, together with a much lower one ascribed to the copolymer in molecular form. On increasing the concentration, the two components tend to disappear because micelles, which are being formed, dissolve the impurities. Moreover, Zhou and Chu [41] observed that an anomalous association process takes place in commercial PEO-PPO-PEO block copolymers, in presence of impurities. The latter manifest themselves with the presence of a peak in the I(T) and R_{app}(T) values close to the CMT. As observed in Figs. 4 and 5, no such anomalies take place in the present case and no impurities occur.

Below 35 °C, the analysis of the intensity–intensity time autocorrelation function by the constraint-regularized Contin method [42] gives a single peak of the intensity-weighted distribution for the hydrodynamic radii $P(R)$, Fig. 6. R_{app} values of about 2.1 nm are obtained in such temperature range. In view of these results, I and R_{app} values are reasonably ascribed to the mass and to the hydrodynamic radius, respectively. Above the CMT, however, both molecules and micelles contribute to I and R_{app} values. This hypothesis is supported by the $P(R)$ distribution function. In Fig. 7, the molecular and micelle peaks, at about 2.1 and 6.5 nm, respectively, are observed. On increasing T, the self-association proceeds, and an increase in the micelle peak intensity is observed.

The contribution of each species to $P(R)$ is proportional to the fraction of scattered intensity, i.e. to the respective concentrations and molar masses. Of course, the molecular molar mass is much lower than the aggregate one. This means that, even when the concentration of the two species is comparable, the scattered intensity component of the molecular species is much lower and becomes negligible from 50 °C upwards. Hence, the molecular peak disappears from the $P(R)$ pattern, and an almost constant R_{app} is obtained (Fig. 4). Nevertheless, the total scattered intensity keeps on growing with temperature. This behaviour is

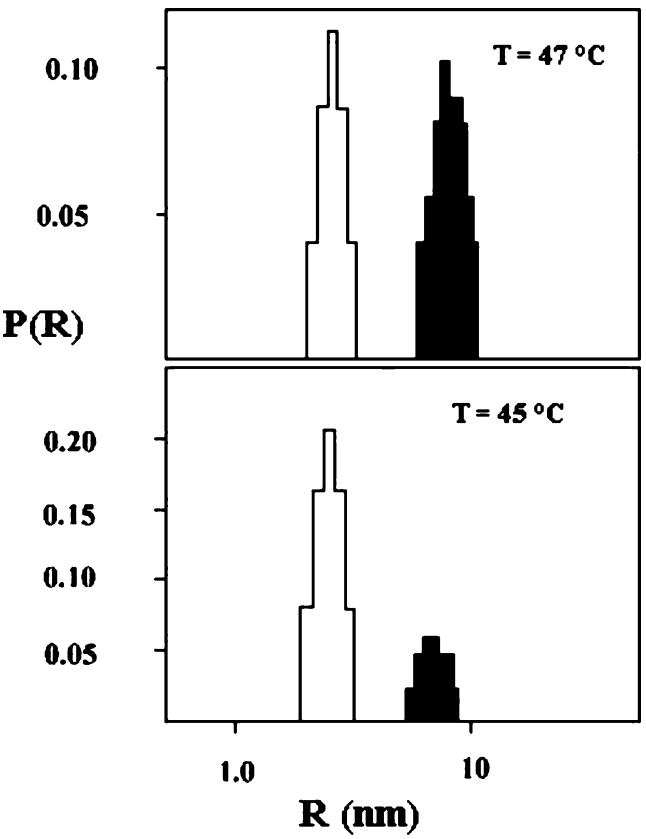

Fig. 7 The intensity weighted distribution, $P(R)$, in arbitrary units as a function of R_{app}, in nm, slightly above the CMT. The solution contains 5.02 F68%. The integrals are proportional to the scattering contributions due to molecules, *left*, and micelles, in *black*

observed also in the I pattern reported in literature on similar systems [43]. In our opinion, it indicates that a significant amount of free molecules is still present in solution above 50 °C and keeps on self-associating, thus increasing the overall scattered intensity. Moreover, even if the average micelle size does not change much, a partial desolvation of the PPO residues and an increase in aggregation numbers can take place concomitantly and account for the aforementioned intensity patterns.

Nuclear magnetic resonance

At room temperature, the ^{1}H spectra of F68 show a sharp singlet, due to methylene units (at 3.74 ppm), and a partial overlapping of signals due to methyl and methyne groups (the CH one) at 1.22 ppm [29, 30]. Modifications in position, line width and spin-lattice relaxation times, T_1, are associated with the behaviour of the polar or non-polar region, respectively. The spectrum of F68 is simple, and modifications in the relaxation processes of the polar and nonpolar regions come out univocally from experiments.

As a consequence of micelle formation, the PEO and PPO portions of F68 undergo significant changes in hydration. Both domains change, presumably, their conformational degrees of freedom. This is evident in ^{1}H NMR spectra as a function of temperature, inset in Fig. 8. In particular, significant changes in the peak's shape, chemical shifts and spectral profiles of methyl and methyne protons are observed. At low temperatures, the resonance peak splits in two because of the coupling of CH_3 proton signal with the CH one. Above the CMT, the CH_3 signal is 0.08-ppm high field shifted. At the same time, a significant line broadening is observed, and the doublet disappears. Modifications in the relaxation processes of methyl groups above the CMT imply variations in PPO chain packing [44, 45], consequent to micelle formation (Fig. 8).

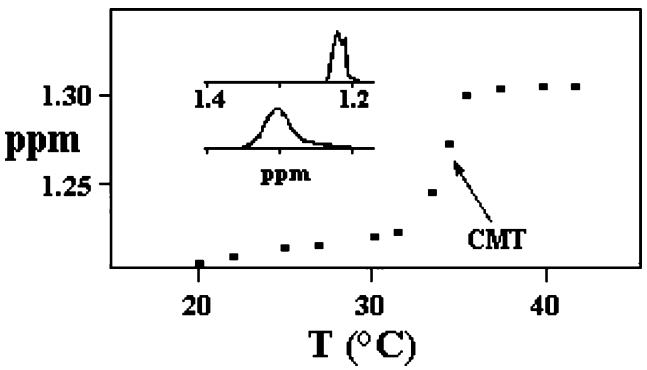

Fig. 8 Chemical shift of the methyl group in the oxy-propylene units of F68, in ppm, for a 10.08 F68% mixture in D_2O as a function of T (°C). In the *inset* are reported the methyl (plus methyne) group line shape at 22.0 °C, *top*, and 37.5 °C

NMR self-diffusion supports former LS findings and indicates the occurrence of molecular or micellar regimes. These are separated by sudden changes in slope, or small discontinuities, and depend on F68 content. The R_H results obtained from NMR, by using the Stokes–Einstein equation, are consistent with those from LS in the temperature range where the molecular regime occurs and a comparison between z-average and number average statistics is possible [27]. In that case, the polydispersity is only ascribed to the distribution of molecular masses. In the molecular regime, typical hydrodynamic radii inferred by NMR self-diffusion are 1.8–2.0 nm.

Spin-lattice relaxation times are a powerful tool to investigate the micro-dynamics of such systems. An example is given in Fig. 9, where the relaxation times of CH_3 and oxyethylene (EO) protons are reported as a function of $1/T$. At low temperatures, T_1 values of EO and methyl units in oxypropylene (PO) groups are superimposable. The curve relative to the latter groups changes in slope from the CMT upwards, and the relaxation time becomes faster on increasing T. The slope of $T_1(T)$ curves contains information on the energy barriers controlling the relaxation mechanism. The activation energy of the above processes was calculated by a Debye-like equation, according to [46, 47]

$$\ln\left(T_1(T)\right) = \ln\left(\frac{h}{k}\right) - \left(\frac{\Delta S_{att}}{R}\right) + \left(\frac{\Delta H_{att}}{RT}\right) \qquad (6)$$

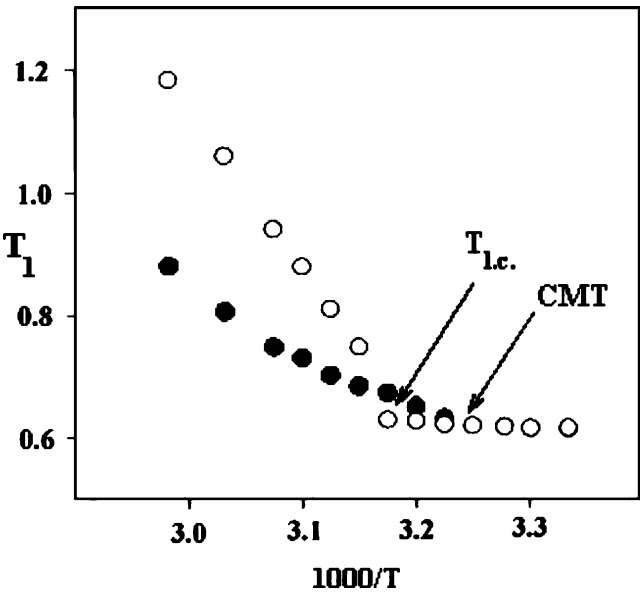

Fig. 9 The spin-lattice relaxation time, T_1, (s), vs $10^3/T$, ($°C^{-1}$), for methyl, (*filled circles*), and oxy-ethylene, (*open circles*), protons of a 36.67 F68% mixture in D_2O. The CMT and the liquid crystalline phase transition, T_{tr}, occur at the respective changes in slope. Below the CMT, the relaxation times of oxy-ethylene and methyl protons in PPO units overlap

where h and k are Planck's and Boltzmann's constants and ΔS_{att} and ΔH_{att} the activation contributions to the process. If the temperature range is moderate, ΔH_{att} can be obtained by

$$\Delta H_{att} = R\left[\frac{d(\ln T_1)}{d\left(\frac{1}{T}\right)} - T\right] \tag{7}$$

The activation enthalpy of T_1 for methyl protons, 10.2 kJ mol^{-1}, is nearly the same in micellar and liquid crystalline form, and its concentration dependence is small. The relaxation mechanisms associated to liquid crystal formation inferred by EO motion are significantly different. In a sample containing 40.06 F68%, for instance, ΔH_{att} values associated to the motion of EO groups are about 18.3± 0.3 kJ mol^{-1}. Above the transition temperature, EO groups are less mobile in liquid crystal than in micelles, as high activation energies imply noticeable hindrance to molecular motion. This behaviour implies the following possibilities:

- Interactions between neighbour aggregates (because the volume fraction required to form bcc phases is close to the phase separation limit) [48, 49];
- Thermal dehydration of EO moieties, due to a decrease in dipole moments of the PEO chains [50].

The latter hypothesis finds analogy with what is observed in high molecular weight PEO in solution [50], or in aqueous alkyl poly(oxy-ethylene) glycols [51], where a thermally induced phase separation is observed. It is not easy "a priori" to determine which effect is dominant. According to the present findings and to SANS [52, 53], both effects are relevant.

Rheology

As a consequence of variations in composition and temperature, significant modifications in the rheological properties occur. Dramatic changes in G' and G'' values are observed when the molecule–micelle and the micelle–liquid crystal transitions are approached (Fig. 10). The micelle–liquid crystal phase transition is not much sensitive to ω or thermal scans. The temperature at which the rheological properties reach the second plateau (Fig. 10) is the micelle–liquid crystal transition. Changes in G' values associated to the former transition are three orders of magnitude high, those related to the micelle–liquid crystal transition one or two. The same holds for G'' values.

Large changes in the system viscosity occur because, presumably, micelle entanglement takes place. The effect is significant at high F68 content for volume fractions higher than 0.2 Φ, and spatial correlation between aggregates may occur, as formerly inferred by SANS [12]. At high

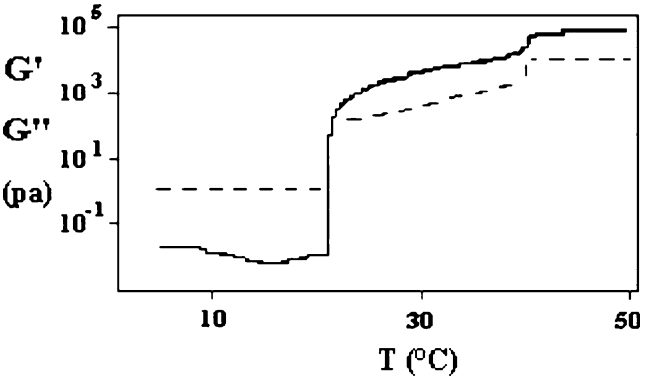

Fig. 10 Dependence of G' (*full*) and G'' (*dashed line*), (Pa), on T, (in °C), for a solution containing 39.76 F68%. The applied frequency is 6.283 rad s^{-1}, when the thermal scan speed 1.5 °C min^{-1}

frequencies, small, or no, visco-elastic effects are observed in the molecular and the micellar region. For low frequency stresses, conversely, a solid-like behaviour is observed when Φ is above 0.2. This fact supports the hypothesis that micelles self-organise into clusters during the viscous flow.

Data in Fig. 10 are an example of "dynamic" thermal transitions from liquid-like ($G'' \gg G'$) to solid-like regimes ($G' \gg G''$) [54]. The two curves intersect at the molecule–micelle transition temperature. In polymer solutions, the intersection point between G' and G'' curves is the gelation temperature, T_{G} [55]. At present, we do not know whether this is a coincidence, or the result of a more general behaviour, related to the supra-molecular association of block copolymers.

Significant differences between micellar solutions and the liquid crystalline phase are observed by creep tests. The creep compliance, $Q(t)$, is defined as [56]

$$Q(t) = \frac{\gamma(t)}{\sigma} \tag{8}$$

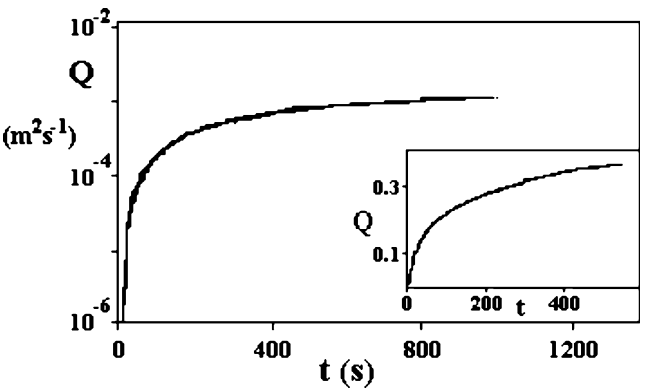

Fig. 11 The creep compliance, Q, (m^2 N^{-1}), vs perturbation time, (s), for a 46.60 F68% sample at 40 °C, in liquid crystalline form. The applied stress is 80 Pa. In the *inset* is reported the behaviour of a 20.40 F68% micellar solution, at 55 °C and 5 Pa applied stress

where σ is the shear stress applied to the system and maintained for the whole duration of the experiment. The deformation, $\gamma(t)$, is monitored as a function of time. The dependence of $Q(t)$ on time indicates whether the system is Newtonian or shows delayed deformation recovery. In steady creeping regime for visco-elastic fluids, the following equality holds [57]:

$$Q(t) = Q_1^{\circ} + \frac{t}{\eta^{\circ}} \tag{9}$$

where Q_1° is the creep compliance in steady state and η° the low-shear viscosity.

The shear rate inferred from the above equation is the slope of the deformation vs time curve. As can be seen in Fig. 11, different dynamic regimes occur in cubic phases. Each of them is characterised by a different time response. At least three different time domains can be inferred by deconvolution of the creep compliance. At low scan rates, a solid-like behaviour occurs due to the extremely high value of the elastic modulus and associated to the aggregates packing in a cubic arrangement. In such conditions, aggregates are significantly hindered; this is reflected not only in rheology but also in ^{2}H NMR and in the high activation barriers to EO chains motion.

In micellar solutions, conversely, the visco-elastic behaviour is ascribed to micelle entanglement in fair good agreement with light and neutron scattering [12, 16]. The kinetics of the molecule to micelle transition may be significantly modified. This hypothesis implies the occurrence of slow visco-elastic relaxation effects associated to the micellization of F68 [58].

Conclusions

The purpose of this contribution is to shed light on some modifications in the physical properties associated to micelle and liquid crystal formation for a block copolymer. Changes in the observed quantities are related to the association of F68 into micelles or to the formation of a bcc phase. The timescale under investigation allows one to observe different processes. Thanks to its high HLB value, the molecule–micelle equilibrium of F68 occurs at relatively high temperatures compared to other members of the Pluronics family. And its polymorphic behaviour is quite moderate.

Rheological methods give information on modifications in the overall system structure subsequent to shear stresses. These results depend on the physical state, local dynamics and structure of the organised domains. Micelle–micelle interactions modulate the system response to shear stresses and are responsible for collective motions in the system. T_1 values, conversely, give information on the system response during local scale motions. The two effects are interrelated.

The dehydration of different molecular moieties in the copolymer is strongly and selectively dependent on temperature. PO dehydration controls the segregation of less polar groups into micelles and occurs at low T values. Dehydration of EO groups, conversely, occurs at higher temperatures. According to the present results, EO dehydration is concomitant to the squeezing phenomena observed in micelles and controls inter-micellar interactions, with consequent packing into liquid crystalline phases. Both hypotheses are in fair good agreement with former studies [11, 12].

Information on micelle size and shape, as well as on hydration, of Pluronics have been published in the past, but much less is known on the local dynamic properties sensed by the hydrophilic and lipophilic groups during micelle or liquid crystal formation. It was shown that the energy barriers hindering the motion of EO groups are higher than those responsible for the PO units.

The increase in particle size with temperature has been clarified, and the occurrence of two scattering populations has been demonstrated by a Contin analysis. No anomalous increase in particle size close to CMT was observed [40]. At the same time, the thermal transitions from molecular to micellar form have been studied in detail by rheological methods. Despite the relatively small increase in particle size (inferred by LS), the real and imaginary components of the complex viscosity significantly changed in proximity of the molecule–micelle thermal transitions. This effect is, in some aspects, unexpected and may be rationalised in terms of micelle–micelle interactions mediated by interconnections between micelles. It becomes significant at moderately high volume fractions. According to Zhou and Chu [11, 12], as well as to recent findings by Lindner et al. [49], this behaviour is presumably related to volume fraction effects when heavily hydrated aggregates are partly hindered in their motion.

Acknowledgement Some results presented in this paper were included in the M.S. thesis of S. P., in partial fulfillment of requirements for her graduate thesis on Chemistry, University of Rome “La Sapienza”. MIUR is acknowledged for financial support, through a COFIN on Polymer-Surfactant Systems, (2002–2004), no. 2002037154-001. Prof. G. A. Ranieri and Dr. C. Oliviero, Department of Chemistry at Calabria University, are gratefully acknowledged for use of the low-resolution NMR unit.

References

1. Bahadur P, Ries G (1996) Tenside Surfactants Deterg 28:173
2. Alexandridis P, Hatton TA (1994) Colloids Surf A 27:2414
3. Schmolka JR (1986) Cosmet Toiletries 99:69
4. Schmolka JR (1977) J Am Oil Chem Soc 54:110
5. Kunieda H, Shigeta K, Suzuki M (2000) Langmuir 15:3118
6. Kunieda H, Kabir H, Aramaki K, Shigeta K (2001) J Mol Liq 90:157

7. Alexandridis P, Olsson U, Lindman B (1998) Langmuir 14:2627
8. Svensson B, Olsson U (2000) Macromolecules 33:7413
9. La Mesa C (2000) J Therm Anal Calorim 61:493
10. Gente G, Iovino A, La Mesa, C (2004) J Colloid Interface Sci 274:458
11. Chu B, Zhou Z (1996) In: Nonionic surfactants, Surf. Sci. Ser., vol. LX. Marcel Dekker, New York, p 67
12. Zhou Z, Chu B (1988) J Colloid Interface Sci 126:171
13. Yu GE, Deng Y, Dalton S, Wang QG, Attwood D, Prince C, Booth C (1992) J Chem Soc, Faraday Trans I 88:2537
14. Alexandridis P, Olsson U, Lindman B (1992) Macromolecules 28:7700
15. Alexandridis P, Holmqvist P, Olsson U, Lindman B (1997) Colloids Surf A 129:3
16. Svensson B, Olsson U, Alexandridis P, Mortensen K (1999) Macromolecules 32:6725
17. Davies JT, Rideal EK (1963) Interfacial phenomena, 2nd edn. Academic, London
18. BASF Corp (1996) In: Pluronic@ PE types Techn Inform. Parsippany, NJ
19. Gunther H (1996) NMR Spectroscopy, chap. VII, 2nd edn. Wiley, New York
20. Briganti G, Capitani D, Casieri C, La Mesa C, Segre AL (1999) J Phys Chem B 103:825
21. Capitani D, Casieri C, Briganti G, La Mesa C, Segre AL (1999) J Phys Chem B 103:6088
22. Coppola L, La Mesa C, Ranieri GA, Terenzi M (1993) J Chem Phys 98:5087
23. Muzzalupo R, Ranieri GA, La Mesa C (1996) Langmuir 12:3157
24. Stejskal OS, Tanner JE (1965) J Chem Phys 42:288
25. Tanner JE (1970) J Chem Phys 52:2523
26. D'Archivio AA, Galantini L, Giglio E (1997) Langmuir 13:4197
27. D'Archivio AA, Galantini L, Tettamanti E (2000) J Phys Chem, B 104:9255
28. Koppel DE (1972) J Chem Phys 57:4814
29. Iovino A, (2001) Thesis, "La Sapienza" University, Rome
30. Iovino A, La Mesa C, Capitani D, Segre AL (2003) Colloid Polym Sci 281:1136
31. Macosko CW (1994) Rheology principles, measurements and applications, chap. V. VCH, New York
32. Tanford C (1980) The hydrophobic effect: formation of micelles and biological membranes, chap IV, 2nd edn. Wiley, New York, p 21
33. Mortensen K, Pedersen JS (1992) Macromolecules 25:5440
34. Su Y-L, Wang J, Liu H-Z (2002) Macromolecules 35:6426
35. Guo C, Wang J, Liu H-Z, Chen J-Y (1999) Langmuir 15:2703
36. Caragheorgheopol A, Schlick S (1998) Macromolecules 31:7736
37. Mortensen K (1997) Macromolecules 30:503
38. Alexandridis P, Olsson U, Lindman B (1998) Langmuir 14:2627
39. Brown W, Schillen K, Almgren M, Hvidt S, Bahadur P (1991) J Phys Chem 95:1850
40. Almgren M, Van Stam J, Lindblad C, Li P, Stilbs P, Bahadur P (1991) J Phys Chem 95:5677
41. Zhou Z, Chu B (1988) Macromolecules 21:2548
42. Provencher SW (1979) Makromol Chem 180:201
43. Zhou Z, Chu B, Nace VM, Yang Y-W, Booth C (1996) Macromolecules 29:3663
44. Hunter PN, Sceutejents JMHM, Hatton TA (1993) Macromolecules 26:5592
45. Hansson P, Joensson B, Stroem C, Soederman O (2000) J Phys Chem B 104:3496
46. Hasted JB, (1993) In: Franks F (ed) Water. A comprehensive treatise, chap. VII, vol. 2. Plenum, New York, p 405
47. Hasted JB (1973) Aqueous dielectrics, chap. III. Chapman & Hall, London
48. Chen S-H, Liao C, Fratini E, Baglioni P, Mallamace F (2001) Colloids Surf A 183:95
49. Lindner H, Scherf G, Glatter O (2003) Phys Rev, E Stat Nonlin Soft Matt Phys 67:402
50. Karlstroem G (1985) J Phys Chem 89:4962
51. Weckstrom K, Zulauf M (1985) J Chem Soc Faraday Trans I 81:6033
52. Borbély S (1998) Physica B 241–243:1016
53. Borbély S (2000) Physica B 276–278:363
54. Shigeta K, Olsson U, Kunieda H (2000) Langmuir 17:4717
55. Liu Y (1998) Rheol Acta 38:357
56. Prud'homme RK, Wu O, Schneider DK (1996) Langmuir 12:4651
57. Whorlow RW (1992) Rheological techniques, 2nd edn. Ellis Horwood, London
58. Cabana A, Aif-Kadi A, Juhasz J (1997) J Colloid Interface Sci 190:307